Influence of air pressure on the performance of plasma synthetic jet actuator*

Yang Li(李洋)[1], Min Jia(贾敏)[1], Yun Wu(吴云)[2,†], Ying-hong Li(李应红)[1], Hao-hua Zong(宗豪华)[2], Hui-min Song(宋慧敏)[1], and Hua Liang(梁华)[1]

[1] *Air Force Engineering University, Xi'an* 710038, *China*
[2] *Xi'an Jiaotong University, Xi'an* 710049, *China*

(Received 29 September 2015; revised manuscript received 14 April 2016; published online 19 July 2016)

Plasma synthetic jet actuator (PSJA) has a wide application prospect in the high-speed flow control field for its high jet velocity. In this paper, the influence of the air pressure on the performance of a two-electrode PSJA is investigated by the schlieren method in a large range from 7 kPa to 100 kPa. The energy consumed by the PSJA is roughly the same for all the pressure levels. Traces of the precursor shock wave velocity and the jet front velocity vary a lot for different pressures. The precursor shock wave velocity first decreases gradually and then remains at 345 m/s as the air pressure increases. The peak jet front velocity always appears at the first appearance of a jet, and it decreases gradually with the increase of the air pressure. A maximum precursor shock wave velocity of 520 m/s and a maximum jet front velocity of 440 m/s are observed at the pressure of 7 kPa. The averaged jet velocity in one period ranges from 44 m/s to 54 m/s for all air pressures, and it drops with the rising of the air pressure. High velocities of the precursor shock wave and the jet front indicate that this type of PSJA can still be used to influence the high-speed flow field at 7 kPa.

Keywords: plasma synthetic jet actuator, air pressure, performance, schlieren method

PACS: 52.50.Dg, 52.80.Mg, 52.80.Vp, 47.80.Jk **DOI:** 10.1088/1674-1056/25/9/095205

1. Introduction

Nowadays, plasma aerodynamic actuators have been widely investigated in the active flow control field, including surface dielectric barrier discharge plasma actuators, microwave discharge plasma actuators, and so on.[1,2] With the advantages of no mechanical moving parts, simple structure, flexible control, high actuation frequency, rapid response, and reliable working capacity, these actuators have shown a successful and effective application in the low-speed flow field, such as the stall separation control and the aircraft performance enhancement.[3] However, as for the supersonic and hypersonic flow control, a poor control capacity and indistinctive control effect are demonstrated by using the above actuators.

In order to improve the supersonic flow control effect, a new type of plasma aerodynamic actuator called a plasma synthetic jet actuator (PSJA) has been developed by John Hopkins University.[4] It combines the pin to pin discharge with the synthetic jet technology together and its working period usually includes three stages. In the first stage, the air in the cavity is heated quickly by arc discharge, and both the air temperature and pressure increase rapidly. In the second stage, the air in the cavity is injected into the surrounding environment. In the third step, the continuous injection produces a local vacuum in the cavity and draws the fresh air back into the cavity, waiting for the next working period.[5] PSJA has attractive characteristics of zero net mass flow, simple structure, flexible control, and fast response. Most importantly, it can produce a high speed jet, thus showing a promising application in the supersonic flow control.[6]

Currently, two main parameters affecting the PSJA performance are widely investigated. One is called the structural parameters including the cavity volume, the orifice diameter, and so on. The other called the electric parameters usually constitutes discharge type, applied voltage, actuation frequency, pulse energy, and so on. Many methods (such as high speed schlieren system, pressure sensor, and particle image velocimetry) have been adopted to investigate the PSJA performance (jet field, jet velocity, and pressure in the cavity).[7,8] Cybyk *et al.* investigated the influence of the actuator geometrical parameters on the performance of PSJA through experiments and numerical simulations. The results show that with the increase of the volume, the peak jet front velocity and the jet duration decrease. The bigger the orifice diameter is, the shorter the jet duration will be.[9–11] Compared with PSJA driven by inductive power supplies (IPS), the PSJA driven by capacitive power supplies (CPS) has a higher energy deposition rate and a more powerful jet with higher velocity and shorter expulsion time. Besides, it heats the gas less significantly than the IPS.[12,13] A larger discharge size leads to a higher jet front velocity and a higher precursor shock wave velocity.[14] Below 400 Hz, the jet front velocity remains unchanged, while it decreases when the frequency exceeds 500 Hz.[15] Santhanakrishnan *et al.* investigated the pulsing

*Project supported by the National Natural Science Foundation of China (Grant Nos. 51407197, 51522606, 51336011, 91541120, and 11472306).
†Corresponding author. E-mail: wuyun1223@126.com
© 2016 Chinese Physical Society and IOP Publishing Ltd

frequency on the jet characteristics experimentally and found that the maximum velocity was obtained in the 10 Hz range among three different frequencies (1 Hz, 10 Hz, and 100 Hz) in quiescent flow.[16,17] Capacitors with three different capacitances were used to investigate the influence of the capacitance on the performance of PSJA. The results show that with the capacitance rising, the penetration depth, the exhaust time, and the jet velocity increase, with a maximum jet velocity of 495 m/s.[18–22] Moreover, Zong *et al.* studied the influence of the capacitor energy on the jet front velocity, the jet duration time, and the jet affected area. With the increase of the capacitor energy, the jet front velocity always goes up, while the jet duration time first increases and then keeps constant. The jet affected area has the same change law with the jet duration time.[23,24]

In those researches, the working pressure, a rather significant parameter influencing the PSJA performance, was not quantitatively analyzed. Emerick *et al.* studied the PSJA characterizations in quiescent and supersonic flowfields. For a single-orifice actuator, the maximum blast wave reached 400 m/s. The jet front velocity at 60 kPa was 310 m/s, while it was 240 m/s at 100 kPa.[25] Wang *et al.* investigated the effect of the pressure on the performance of PSJA.[26,27] The results show that the breakdown voltage, the discharge current, and the energy deposition are higher for higher air pressure levels; the peak jet front velocity and the precursor shock wave velocity reach approximately 460 m/s and 530 m/s respectively by the pressure conditions. However, the extension of the air pressure in this research is relatively narrow (10–100 kPa). A wider air pressure on the performance of PSJA should be analyzed. Moreover, the changing processes of the jet front velocity and the precursor shock wave velocity with time for different air pressures need to be exploited.

In this paper, a sequential discharge power supply (nanosecond discharge-capacitive discharge) is adopted to feed a two-electrode PSJA. The influence of the air pressure on the discharge characteristics and the PSJA performance (the flow field evolution, jet front velocity, precursor shock wave intensity, and so on) is investigated with the electrical diagnostic system and the schlieren system, respectively.

2. Experimental setup

2.1. Actuator description

As shown in Fig. 1, a new type of two-electrode PSJA includes two main components: brass nut and ceramic shell. The shell is made of glass ceramic, which has a higher insulation and thermal conductivity. The shell and the nut are fastened together through the thread, so as to form a cavity. On the nut top side, there exists a 1.5 mm orifice drilled as the jet exit where high-temperature and high-pressure air issues out. With a 7 mm height and a 4 mm diameter, the cavity has a volume of 88 mm^3. There are two tungsten needles with a diameter of 1 mm inserted into the cavity. They are used as anode and cathode, respectively. In order to seal the cavity and make the two trigger electrodes discharge in the cavity, temperature-resistant silica gel is used. The distance between the middle of the two electrodes is set as 4 mm, and the two electrodes are 5 mm away from the cavity nut. In this paper, the working period of the two-electrode PSJA consists of four distinct stages which are similar to the traditional three-electrode PSJA, including trigger discharge, energy deposition, air expulsion, and air recovery.

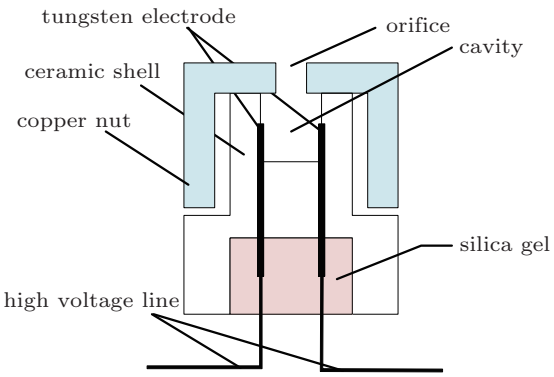


Fig. 1. (color online) Sketch of the actuator.

2.2. Power supply

The power supply system of the two-electrode PSJA in this paper is different from that of the normal two-electrode PSJA. As shown in Fig. 2, the system consists of a high-voltage DC power supply, a high-voltage nanosecond pulsed power supply, two capacitors, a resistor, a magnetic switch, and a signal generator DG535. The maximum output voltage of the high-voltage nanosecond pulsed power supply is 20 kV with a rising time of 2–3 ns and the repetition frequency ranging from 0 to 20 kHz. The anode is connected to capacitor 2, which is linked to the high-voltage pulsed power supply. The high-voltage pulsed power supply is used to create a spark firstly across the anode-cathode gap. At the same time, the anode is connected to the capacitor 1 that is charged by the high-voltage DC power supply. The output voltage of the DC power supply ranges from 0 to 3 kV. The resistor (1000 Ω) is placed between the DC power supply and the capacitor 1 in order to limit the charging current. The magnetic switch and the capacitor 2 are used to separate the high-voltage breakdown circuit from the charge circuit so as to protect both power supplies. In this experiment, the working voltage of the DC power supply is set at 1 kV. Capacitor 1 is 2 μF and capacitor 2 is 2 pF.

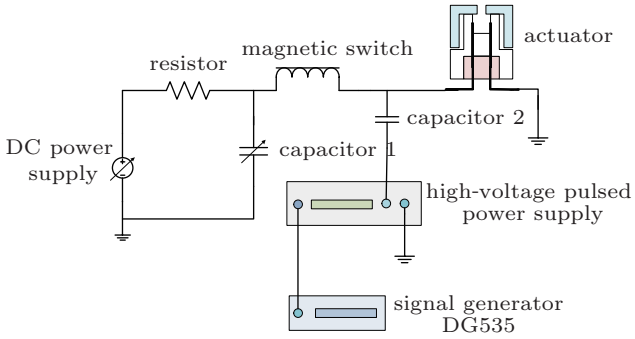


Fig. 2. (color online) Power supply system.

The experimental steps are as follows. Firstly, the DC power supply charges capacitor 1. Next, DG535 generates a TTL trigger signal. Then the high-voltage pulsed power supply receives the signal and produces a high voltage to breakdown the gap between the two electrodes. Finally, the energy stored in capacitor 1 is released until it is difficult to maintain the discharge channel. The operation is in a single pulse mode with the pulsing frequency set at 1 Hz.

2.3. Vacuum chamber

In the experiment, the PSJA is placed in a vacuum chamber. The vacuum chamber has two optical glasses, which makes it easy to detect the jet by the schlieren system clearly. The vacuum chamber is connected to a vacuum pump which can make the pressure in the chamber range from 300 Pa to 100 kPa. In this experiment, the vacuum chamber ambient air pressure ranges from 7 kPa to 100 kPa.

2.4. Measurement systems

2.4.1. Electrical characteristics

In this experiment, the measurement equipment of the electrical parameters includes an oscilloscope (Tektronix DPO4104), a high voltage probe (Tektronix P6015A), and a current probe (Pearson 2878). They are used to measure the applied voltage and the discharge current. The instantaneous discharge power and the total discharge energy are obtained based on the measured voltage and current.

2.4.2. Schlieren system

The flow structure of the plasma synthetic jet is often visualized by the schlieren system, which transforms the density variation into the image brightness. The schlieren system consists of a continuous Xe lamp, two concave mirrors (diameter 30 cm, focus length 1.5 m), a knife, and a high-speed CCD camera (Phantom, V2511). The light emitted from the light source passes through the flow region. The camera is placed after the focal point of the second concave mirror. In order to enhance the image contrast, a knife is put in front of the CCD camera, as shown in Fig. 3.

The high-speed CCD camera used in this research work has the exposure time of 1 μs and the framing rate of 70043 Hz. The air pressure in the vacuum storehouse varies from 7 kPa to 100 kPa.

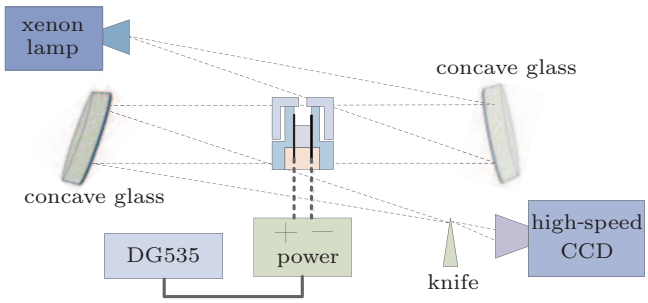


Fig. 3. (color online) Schematic diagram of the Schlieren system.

3. Results and discussion

3.1. Electrical characteristics

Figure 4 shows the applied voltage, the discharge current, and the instantaneous discharge power trace during a discharge at standard air-pressure condition. The discharge waveform at 60–90 kPa is similar to that shown in Fig. 4. Because the magnetic switch has a large inductance, capacitor 1, the inductor (magnetic switch), and the arc gap constitute an *RLC* oscillating circuit. As shown in the figure, when the gap between the two electrodes is broken down, the voltage drops quickly and experiences a drastic oscillation. After approximately 90 μs, the voltage keeps at 300 V. The current goes up to a maximum of 240 A at $T = 7$ μs, and then decreases to 0 A at $T = 18$ μs. After 30 μs, the current drops to −190 A, and the corresponding voltage drops to −180 V. The air in the cavity is heated again. Namely, there are two discharge phenomena among a discharge process, which can also be found from Fig. 4(b). After the first discharge process, the electrode gap is broken down easily because of the existence of residual arc plasma and hot air in the cavity. So when the voltage drops to −300 V, another discharge process takes place. During the whole discharge process, the averaged discharge power reaches 17 kW. The discharge power density is estimated to be 193 W/mm^3, which implies that the air in the cavity will be heated.

Figure 5 shows the applied voltage, the discharge current, and the instantaneous discharge power trace during a discharge at 30 kPa. The discharge waveform at 7–50 kPa is similar to that at 30 kPa. Compared with the discharge voltage waveform at 100 kPa, the voltage experiences a more drastic oscillation at 30 kPa. After approximately 125 μs, the voltage keeps at −200 V. The gap of the two electrodes is broken down three times, so the air in the cavity is heated three times, which can also be discovered from Fig. 5(b). After the first discharge process, there still exists residual arc plasma across the two electrodes, therefore the gap can breakdown easily. When the

voltage decreases to −300 V, the cavity experiences discharge again. Since the electrode gap is broken down more easily for low air pressure levels, the third discharge only initiates below 50 kPa.

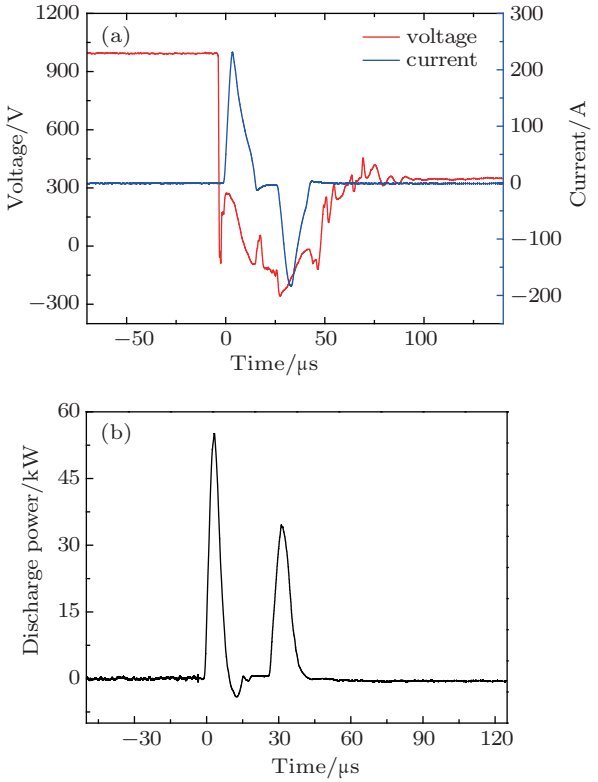


Fig. 4. (color online) Discharge characteristics at 100 kPa: (a) waveforms of the applied voltage and the discharge current, (b) discharge power trace.

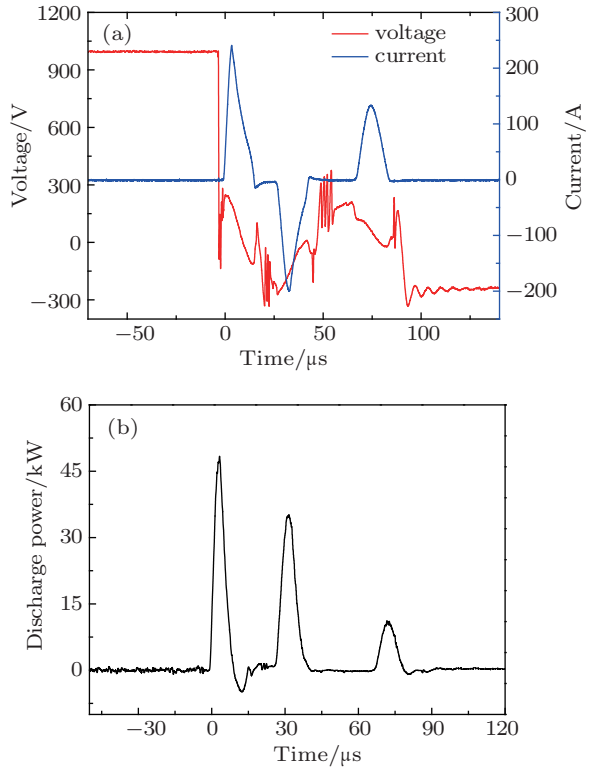


Fig. 5. (color online) Discharge characteristics at 30 kPa: (a) waveforms of the applied voltage and the discharge current, (b) discharge power trace.

Figure 6 shows the relationship between the discharge energy and the air pressure. For all the pressure levels, the discharge energy almost remains constant because the discharge type is still arc discharge instead of glow discharge. In a discharge cycle, the arc energy consumed between the two electrodes E_b and the capacitor 1 energy E_c can be calculated as

$$E_b = \int_0^T u_b(t) i_b(t)\,dt,$$
$$E_c = 0.5 C_1 U_0^2, \quad (1)$$

where $u_b(t)$ and $i_b(t)$ represent the discharge voltage and the current measured by the high voltage probe and the current probe, respectively, C_1 is the capacitance of capacitor 1, and U_0 is the voltage on capacitor 1. As shown in the picture, the arc energy consumed between the two electrodes is about 500 mJ. The energy deposited in capacitor 1 is 1000 mJ, so the arc discharge energy corresponds to 50% of the capacitor 1 energy.

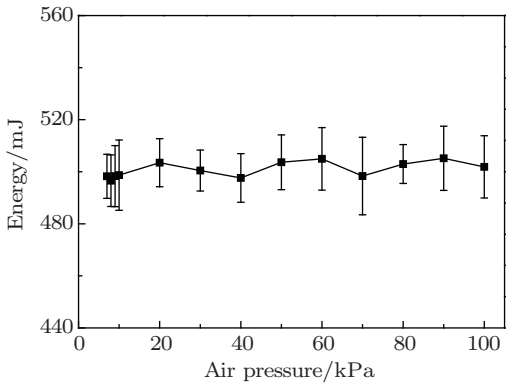


Fig. 6. Discharge energy for different air pressures.

3.2. Schlieren imaging

The jet evolution patterns for different air pressures (7 kPa, 30 kPa, 40 kPa, 70 kPa, and 100 kPa) and different time (14.3 μs, 42.9 μs, 100.1 μs, 214.5 μs, 443.3 μs, and 900.9 μs) are shown in Fig. 7. Comparing the schlieren images of the same air pressure at different time, the conclusion can be drawn that for high air pressure, both the shock wave and the vortex pair are induced initially, as shown in Fig. 7(a). The jet connected to the vortex begins to expel at $T = 14.3$ μs. The jet penetrated length and affected area spread gradually with time, as shown in Figs. 7(a)–7(f). The induced jet closed to the orifice becomes very thin after $T = 228.8$ μs, indicating that the jet strength weakens gradually. In low air pressure conditions, both the weak shock wave and the jet appear at $T = 14.3$ μs, but there is no obvious vortex below 40 kPa. The jet velocity is higher than that of the surrounding air near the orifice, so there is a high velocity gradient between the jet and the surrounding air. Because of the strong shear between the jet and the surrounding air, the vortex close to the orifice is induced. While below 30 kPa, the air is rare, the shear is poor,

so there is no obvious vortex close to the orifice. The jet penetrated length and affected area are enlarging with time. With the increase of the air pressure, the jet affected area and the jet mass also increase. Additionally, the shock wave brightens up, indicating a rising intensity. The jet penetrated depth at low pressure is longer than that at high pressure.

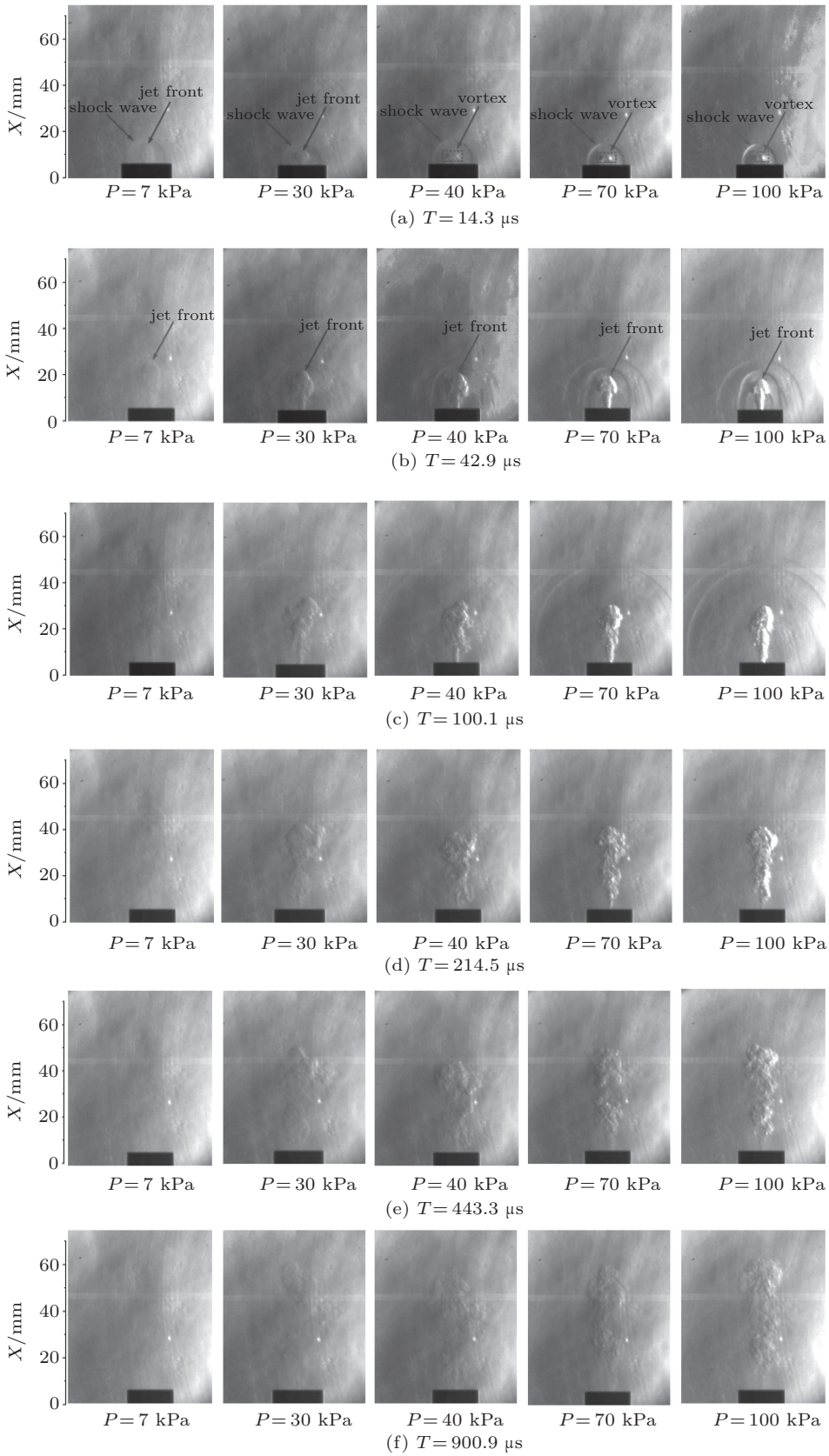


Fig. 7. Schlieren images of the flow field: (a) $T = 14.3$ μs, (b) $T = 42.9$ μs, (c) $T = 100.1$ μs, (d) $T = 214.5$ μs, (e) $T = 443.3$ μs, (f) $T = 900.9$ μs.

As shown in Fig. 7(a) at 7 kPa and Fig. 7(b) at 40 kPa, 70 kPa, and 100 kPa, the precursor shock wave and the second shock wave are ellipsoidal. The calculation results show that the time interval between the precursor and the second shock wave is approximate 25 μs, corresponding to the first two discharges in the discharge power trace. With the increase of time, the distance between the precursor shock wave and the second shock wave decreases gradually.

3.3. Jet front velocity and shock wave velocity

The jet front velocity and the precursor shock wave velocity at different time can be calculated based on the positions of the jet front and the shock wave in the flow field. The accuracy depends on the image resolution and the image interval. In the experiment, the resolution of the schlieren images is 0.14 mm/pixel, and the interval is about 14.3 μs. In order to improve the data accuracy, five results acquired in the same conditions are averaged.

The variations of the jet front velocity for different air pressures are shown in Fig. 8. At 7 kPa and 30 kPa, the jet front velocity drops sharply from 440 m/s to 350 m/s and from 395 m/s to 285 m/s respectively at $T = 14.3$ μs. From 28.6 μs to 42.9 μs and from 71.5 μs to 85.8 μs, the jet front velocity increases because the air in the cavity is heated again, as shown in Fig. 5. After 85.8 μs, the jet front velocity drops gradually. Finally, it keeps at 45 m/s ($T = 200$–300 μs). Because the jet is hard to identify after 300 μs, only the jet velocity before 300 μs at low pressure is presented. At 50 kPa, the jet front velocity gradients at $T = 42.9$ μs and 85.8 μs become small comparing to the surrounding velocity gradient. The cavity experiences discharge again at $T = 42.9$ μs and 85.8 μs, so the air in the cavity is heated again. However, the jet velocity increasing rate caused by heating is lower than the decreasing rate resulting from diffusion, so the jet velocity still decreases slowly. At 100 kPa, the jet velocity decreases sharply before 160 μs, after 160 μs, it keeps at 40 m/s. No matter whether at high pressure or at low pressure, the peak jet front velocity always appears at the first image. The high jet front velocity at low pressure proves that PSJA has the potential to control the shock wave and boundary layer interactions and weaken the strength of the shock wave. It is possible to produce a sufficient aerodynamic force by PSJA to control the flight attitude and thus replace the traditional control surface.

For different air pressure levels, the variations of the peak jet front velocity are shown in Fig. 9. The peak jet front velocity drops very sharply at low pressure. From 50 kPa, the peak front jet velocity drops in a nearly linear way. From 7 kPa, the changing rate of the maximum jet velocity starts to drop gradually. At 7 kPa, the peak jet front velocity reaches 435 m/s, which indicates that the plasma synthetic jet still has control authority to the flow field at low pressure. Even though the energy consumed is constant for all air pressure levels, the air density at high pressure is higher than that at low pressure. Comparing with that at high air pressure, the assigned energy per unit mass at low pressure is higher. Therefore, the peak velocity drops gradually with the increase of the air pressure.

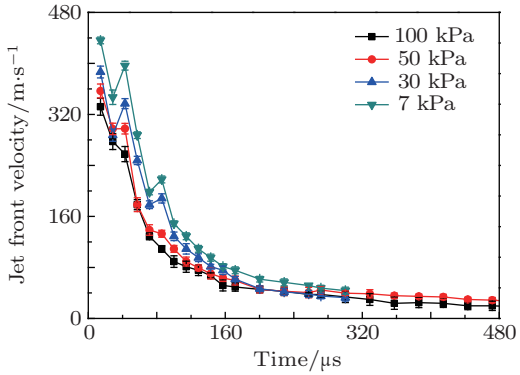


Fig. 8. (color online) Jet front velocity for different air pressures.

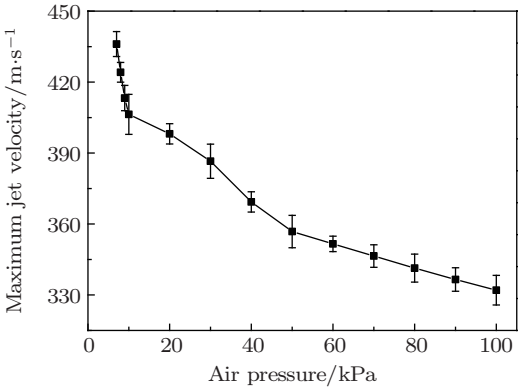


Fig. 9. Variation of the maximum jet velocity with the air pressure.

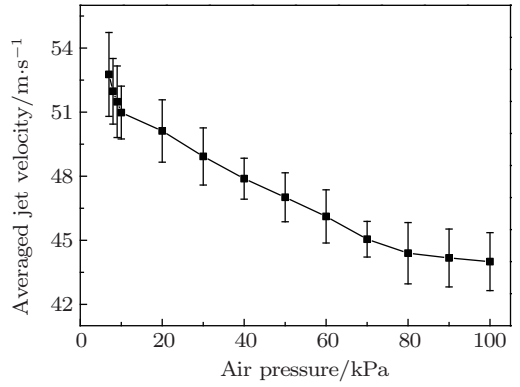


Fig. 10. Variation of the averaged jet velocity with the air pressure.

Figure 10 shows the averaged jet velocity in the first 900.0 μs for different air pressures. The changing rule of the averaged jet velocity is similar to that of the maximum jet velocity. At 7 kPa, the averaged jet velocity reaches 53 m/s,

while it is 44 m/s at 100 kPa. With the increase of the air pressure, the averaged jet velocity decreases gradually. Before 10 kPa, the averaged jet velocity decreases in a rate of 0.7 m/(s·kPa). From 10 kPa to 80 Kpa, the rate of decrement is 0.1 m/(s·kPa). After 80 kPa, the averaged jet velocity nearly remains unchanged.

For different air pressures (7 kPa, 30 kPa, 50 kPa, and 100 kPa), variations of the precursor shock wave velocity are shown in Fig. 11. The precursor shock wave velocity gradually decreases with time. From $T = 80$ μs, the shock wave velocity keeps at 345 m/s. The peak precursor shock wave velocity drops by degrees with the increase of the air pressure. The air temperature close to the orifice is much higher than that of the surrounding air, and the hot air transmits energy to the cold one. Along the jet direction, the air temperature and the changing rate of the air temperature decrease by degrees. The distance between the shock wave and the orifice increases gradually. So the biggest shock wave velocity always appears in the beginning, and the decrease rate of the precursor shock wave is also biggest in the beginning. The air temperature changes very slightly along the horizontal direction, and the shock wave velocity along that direction almost keeps at 345 m/s. The shock wave velocity along the jet direction is higher than that along the jet vertical direction. So the precursor shock wave in Figs. 7(a)–7(c) and the second shock wave in Figs. 7(b) and 7(c) are ellipsoidal.

The high jet front velocity, the high jet averaged velocity, and the high shock wave velocity provide the strongest evidence that PSJ still has a control force at low pressure and a wide application prospect in the high-speed flow control field.

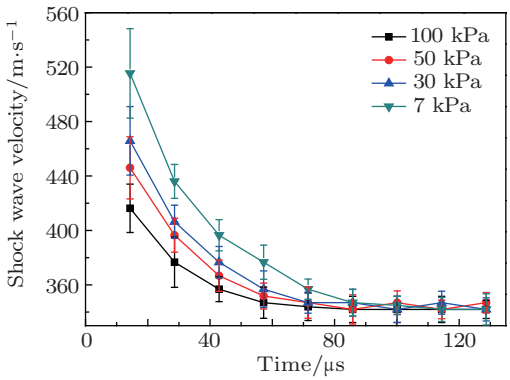
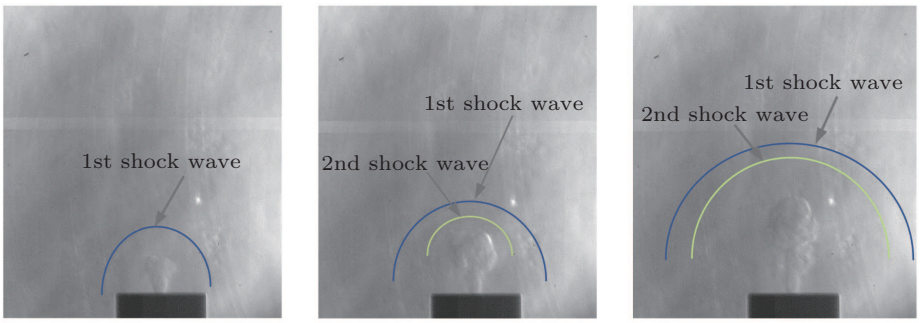
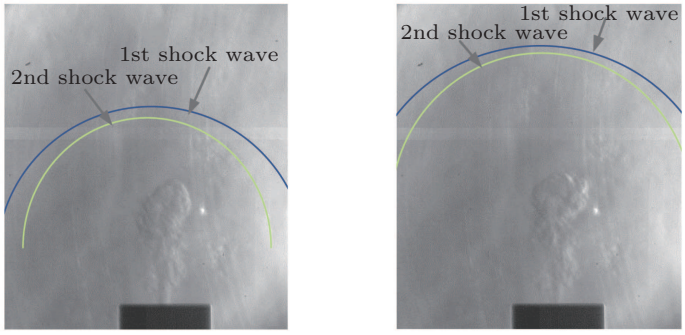


Fig. 11. (color online) Shock wave velocity for different air pressures.

As shown in Fig. 7, the distance between the precursor shock wave and the second shock wave is smaller with the increase of time. In order to display this phenomenon clearly, a group of schlieren images at 30 kPa are presented in Fig. 12, and the locations of the precursor and the second shock waves at different times are marked. The first shock wave appears at $T = 14.3$ μs, and the second shock wave appears at $T = 42.9$ μs. The distance between the first shock wave and the second shock wave decreases, and their fronts are nearly overlapped at $T = 128.7$ μs.



(a) $T = 14.3$ μs (b) $T = 42.9$ μs (c) $T = 71.5$ μs



(d) $T = 100.1$ μs (e) $T = 128.7$ μs

Fig. 12. (color online) Variation of precursor and second shock wave locations at 30 kPa with time: (a) $T = 14.3$ μs, (b) $T = 42.9$ μs, (c) $T = 71.5$ μs, (d) $T = 100.1$ μs, (e) $T = 128.7$ μs.

The air temperature decreases along the jet direction. When the distance between the shock wave and the orifice is bigger, the local air temperature and the shock wave speed are lower. Because the distance between the second shock wave and the orifice is smaller than that between the precursor shock wave and the orifice all the time, the second shock wave velocity is always faster than the precursor one. So with the increase of time, the distance between the precursor shock wave and the second shock wave decreases gradually.

4. Conclusion

The influence of the air pressure on the performance of a two-electrode PSJA, including the flow field evolution, the jet front velocity, and the precursor shock wave velocity, is experimentally investigated. The electrical characteristics and the schlieren images are obtained in a large scope of pressure ranging from 7 kPa to 100 kPa.

With the air pressure rising, the discharge energy almost remains constant. The flow field evolution at high pressure is quite different from that at low pressure. At high pressure, the shock wave appears with a vortex pair in the beginning, and the jet keeps in step with the vortex pair. However at low pressure, the jet and the precursor shock wave appear in the beginning while there is no obvious vortex. Besides, the maximum jet propagation distance is longer at low pressure than that at high pressure.

The jet front velocity in a period always decreases at high pressure ($>$ 50 kPa), while a fluctuation of the jet front velocity occurs during its decay at low pressure. The peak jet front velocity decreases gradually with the increase of the air pressure and reaches 440 m/s at 7 kPa. For different air pressures, the precursor shock wave velocity shows a gradual decrease first and then keeps almost constant at 345 m/s. At 7 kPa, the maximum shock wave velocity reaches 515 m/s. The high-speed shock wave and jet at low pressure show that this type of PSJA can still be used to control the high-speed flow field at 7 kPa.

Further research should aim at the characteristic of PSJA at lower pressure and enhance the strength of plasma synthetic jet at low pressure.

References

[1] Li Y H, Wu Y and Li J 2012 *Int. J. Flow Control* **4** 1756
[2] Zhao G Y, Li Y H and Liang H 2015 *Acta. Phys. Sin.* **64** 015101 (in Chinese)
[3] Zhao G Y, Li Y H, Liang H and Han M H 2015 *Exp. Fluids* **56** 1864
[4] Popkin S H, Taylor T M and Cybyk B Z 2013 *J. Hopkins Apl. Tech. D* **32** 404
[5] Cybyk B Z, Wilkerson J T and Grossman K R 2004 *2nd AIAA* Flow Control *Conference,* June 28–July 1, 2004, Portland, Oregon, p. 2131
[6] Grossman K R, Cybyk B Z and VanWi D M 2004 *42nd AIAA Aerospace Sciences Meeting and Exhibit,* January 5–8 ,2004, Reno, Nevada, p. 0089
[7] Ko H S, Haack S J and Land H B 2010 *Flow Meas. Instrum.* **21** 443
[8] Haack S J, Land H and Cybyk B 2008 *4th Flow Control Conference,* June 23–26, 2008, Seattle, Washington, p. 3759
[9] Cybyk B Z, Grossman K R and Wilkerson J T 2005 *43rd AIAA Aerospace Sciences Meeting and Exhibit,* January 10–13, 2005, Reno, Nevada p. 401
[10] Cybyk B Z, Simon D H and Land H B 2006 *44th AIAA Aerospace Sciences Meeting and Exhibit,* January 9–12, 2006, Reno, Nevada, p. 478
[11] Cybyk B Z, Wilkerson J T and Grossman K R 2003 *33rd AIAA Fluid Dynamics Conference and Exhibit,* Orlando 23–26 , Florida, American, p. 3711
[12] Belinger A, Hardy P and Barricau P 2011 *J. Phys. D: Appl. Phys.* **44** 365201
[13] Berlinger A, Naude N and Cambronne J P 2014 *J. Phys. D: Appl. Phys.* **47** 345202
[14] Belinger A, Hardy P and Gherardi N 2011 *IEEE Trans. Plasma Sci.* **39** 2334
[15] Jin D, Li Y H and Jia M 2013 *Plasma Sci. Tech.* **15** 1033
[16] Santhanakrishnan A and Jacob J D 2007 *J. Phys. D: Appl. Phys.* **40** 637
[17] Santhanakrishnan A, Reasor D A and LeBeau R P 2009 *Phys. Fluids 2009* **21** 043602
[18] Reedy T M and Kale N V 2013 *AIAA J.* **51** 2027
[19] Haack S J, Taylor T and Emhoff J 2010 *5th Flow Control Conference,* June 28–July 1, 2010, Chicago, Illinois, p. 4979
[20] Popkin S H, Cybyk B Z and Land III H B 2013 *51st AIAA Aerospace Sciences Meeting,* January 7–10, 2013, Texas, American, p. 0322
[21] Golbabaei A M, Knight D and Wilkinson S 2015 *AIAA J.* **53** 501
[22] Shin J 2010 *Chin. J. Aeronaut.* **23** 518
[23] Zong H H, Wu Y and Li Y H 2015 *Phys. Fluids* **27** 027105
[24] Zong H H, Cui W and Wu Y 2015 *Sensor Actuat. A: Phys.* **222** 114
[25] Emerick T, Ali M Y and Foster C 2014 *Exp. Fluids* **55** 1858
[26] Wang L, Xia Z X and Luo Z B 2014 *Sci. China-Phys. Mech.* **57** 2309
[27] Wang L, Xia Z X and Luo Z B 2014 *Acta. Phys. Sin.* **63** 194702 (in Chinese)